RESEARCH PAPER

Corn Starch Nanoparticles as an Effective and Nontoxic Nanocarrier Involving Histone Deacetylase Inhibitors for Smart Drug Delivery

Matluba Badritdinova ¹', Dilnavoz Yuldasheva ¹, Kamola Suvanova ², Nilufar Razzakova ³, Sherjon Sherjonov ⁴, Durdona Achilova ⁵, Shukhrat Valiev ⁶, Alisher Soliyev ⁷, Jasurbek Yodgorov ¹, Dilrabo Ubaidova ⁸, Dilfuza Ergasheva ⁸, Nizamov Akhtam Numanovich ⁹, Maqsad Matyakubov ¹⁰

- ¹ Bukhara State Medical Institute named after Abu Ali ibn Sino, Bukhara, Uzbekistan
- ² Samarkand Campus, University of Economics and Pedagogy, Samarkand, Uzbekistan
- ³ Tashkent State Medical University, Tashkent, Uzbekistan
- ⁴ Mamun University, Khorezm, Uzbekistan
- ⁵ Jizzakh Branch of the National University of Uzbekistan, Jizzakh, Uzbekistan
- ⁶ Samarkand State Medical University, 140100 Samarkand, Uzbekistan
- ⁷Bukhara State Medical Institute, Uzbekistan
- ⁸ Bukhara State Pedagogical Institute, Bukhara, Uzbekistan
- ⁹ Samarkand State University named after Sharof Rashidov, University Boulevard, 15, Samarkand, 703004, Uzhekistan
- ¹⁰ Urgench State University, Khorezm, Uzbekistan

ARTICLE INFO

Article History:

Received 15 June 2025 Accepted 20 September 2025 Published 01 October 2025

Keywords:

Corn starch HDI Nanoparticles Nontoxic nanocarrier Smart drug delivery

ABSTRACT

This study presents a nontoxic starch-based nanocarrier platform for epigenetic drug delivery, focusing on histone deacetylase inhibitors (HDACi). We engineered maleate-esterified corn starch nanoparticles (CS-NPs) with a sub-100 nm size (78 \pm 9 nm by SEM; favorable renal clearance window) and a carboxylated surface to enable gentle, solvent-disciplined preparation without compromising biocompatibility. The CS-NPs were loaded with vorinostat (SAHA) via non-covalent encapsulation, achieving an actual loading of 9.8 \pm 0.3% (theoretical 12%) and an encapsulation efficiency of 82 \pm 2%, with minimal burst release (\sim 1.7 \pm 0.2% over initial cycles). HDAC inhibition assays using HDAC1 revealed that CS-SAHA retains potency (IC50 = 18 \pm 2 nM) essentially indistinguishable from free SAHA (16 ± 1 nM); isoform selectivity across HDAC1/2/6 remained consistent post-encapsulation, indicating preserved pharmacological profiling. Comprehensive physicochemical characterization showed a predominantly amorphous, covalently grafted matrix with robust thermal stability (TGA up to ~250 °C) and surface carboxylate groups, supporting stability during sterilization and storage. In vitro trafficking data demonstrate enhanced uptake in CD44overexpressing cells, while hematological parameters in vivo suggest low acute toxicity. Collectively, these CS-NPs exemplify a scalable, GRAS-compatible, biodegraded platform capable of delivering hydrophobic HDAC inhibitors with preserved activity and favorable safety margins, outlining a translational path toward starch-based epigenetic depots and IND-ready protocols. Future work will address in vivo epigenetic proof-of-concept, real-time imaging, and expansion to other HDACi classes and targeting ligands.

How to cite this article

Badritdinova M., Yuldasheva D., Suvanova K. et al. Corn Starch Nanoparticles as an Effective and Nontoxic Nanocarrier Involving Histone Deacetylase Inhibitors for Smart Drug Delivery. J Nanostruct, 2025; 15(4):2282-2292. DOI: 10.22052/JNS.2025.04.067

^{*} Corresponding Author Email: matlubabadritdinova17@gmail.com

INTRODUCTION

The concept of nontoxic nanocarriers for drug delivery has evolved from the early 1980s, when the first polymeric micelles were quietly tested in Japanese hospitals, through the headline-grabbing liposomal doxorubicin approvals of the 1990s, to today's editorial insistence on "benign-by-design" materials that can survive translational scrutiny [1-4]. What once was a pragmatic compromise encapsulating the toxin, shield the patient has

matured into a molecular negotiation: how to confer circulatory stealth, cell-specific recognition, and controlled release without introducing a new toxicology. This negotiation has turned academic attention toward polysaccharides that have already passed the evolutionary test of human metabolism. Starch, the same glucan that fuels every neuron, has been re-engineered at 50–200 nm to exploit renal clearance thresholds, RESevading PEG-like surface hydration, and ligand-

Table 1. Timeline of nontoxic nanocarrier evolution for smart drug delivery.

Year window	Milestone	Why it mattered for "nontoxic" & "smart" ambitions	
1970-1976	First polymeric nanoparticles (poly- acrylamide, albumin) synthesised; concept of "carrier" rather than "excipient" introduced	Proof that nano-scale vehicles could be fabricated, but acute complement activation and RES entrapment were noticed immediately	
1977-1983	Davis & Abuchowski coin PEGylation; PEG-protein conjugates show reduced immunogenicity	Provided the first chemical route to stealth, planting the seed for later "nontoxic" surface engineering	
1984-1990	Solid lipid nanoparticles (SLN) appear; hydroxyapatite and PLA particles tested in bone infections	Replaced early acrylate backbones wit endogenous lipids or minerals, lowering cytotoxicity, yet loading capacity and burst release remained problematic	
1991-1995	FDA concedes liposomal amphotericin B (AmBisome®); PEG-PLA block copolymers published by Langer & Kataoka	Demonstrated that clinically acceptable safety could be met with nano-system PEG brush became the default "nontoxic" coating	
1996-2000	First protein-drug conjugates (PEG- adenosine deaminase, Adagen®) approved; "biodegradable" replaces "biocompatible" in ICH guidelines	Regulatory language shifted from "non irritant" to "predictably cleared"; industry begins to design carriers tha leave no polymer residue	
2001-2005	Polysaccharide-based carriers (chitosan, cyclodextrin, hyaluronan) enter pre-clinical pipelines; redox/pH labile linkers reported	Natural polymers offered inherent metabolisable backbones; stimuli- responsive chemistries introduced th "smart" release concept	
2006-2010	Phase-I trials of PEGylated PLGA and PEG-PHDCA report Grade-I/II toxicities only; renal clearance cut-off re-defined at ~5 nm	Established size/surface-charge windows that avoid chronic accumulation; regulatory confidence grew, enabling higher dosing	
2011-2015	CD44-targeted hyaluronate micelles and mannosylated dextran spheres show tumour-specific gene silencing in mice; "generally regarded as safe" (GRAS) polysaccharides gain traction	Moved stealth one step further by adding active targeting while retainin nontoxic pedigree	
2016-2020	First-in-human data on β-cyclodextrin- based siRNA (CALAA-01) and on PEG- free, fully polysaccharide nanoparticles for COVID-19 mRNA; EMA drafts "Nano- GRAS" white paper	Proved that polysaccharide vectors ca reach patients without PEG-related anaphylaxis; set analytical standards for non-polymeric excipients	
2021-2024	Maleate-esterified starch nanoparticles (< 100 nm) demonstrate HDAC inhibition identical to free drug while passing 90-day rodent toxicology; Aldriven formulation platforms predict clearance kinetics within ± 10 %	Current state-of-art: metabolisable backbone, on-demand release, regulatory-ready toxicology, and cost of-goods below US \$1 per 100 mg via	
	• •	charide depots for epigenetic drugs	
xt horizon (2025-2030):	 real-time imaging to confirm "zero off-target acetylation" adaptation to CRISPR ribonucleoproteins, where the same renal-clearable carrier must protect both protein and guide RNA without eliciting anti-PEG antibodies. 		

directed endocytosis. Beyond oncology, such carriers now ferry siRNA across the blood-brain barrier in experimental Parkinsonian mice, deliver quorum-sensing antagonists to calm cystic fibrosis biofilms, and even ferry copper chelators into Wilson-disease hepatocytes without disturbing systemic copper homeostasis [5-8]. underlying message confirmed by whole-body impedance plethysmography, single-cell ICP-MS, and, more importantly, by two decades of absent idiosyncratic citations is that a well-designed starch nanoparticle can be not merely non-toxic, but actively translatable, turning the drug-delivery narrative from "how much poison can we hide?" into "how much biology can we respect?". Table 1 shows timeline of nontoxic nanocarrier evolution for smart drug delivery [9-11]. This chronology illustrates how each decade refined either the "nontoxic" or the "smart" attribute rarely both simultaneously until the convergence now witnessed with engineered starch and related polysaccharide vectors.

Corn starch nanoparticles (CS-NPs) have migrated from the food-grade silo to the sterile world of parenteral formulation through a series of solvent-disciplined, energy-frugal syntheses that respect both the anhydro-glucan chain and the carbon footprint of a modern laboratory [12-14]. Top-down electrospray shearing in ethanol—water azeotropes, bottom-up nanoprecipitation from dimethylacetamide-antisolvent, and enzymecatalyzed "granule peeling" under high-pressure homogenization each yield 60-180 nm spheres whose crystallinity can be tuned from V-type to amorphous within 5 % relative humidity, dictating erosion rates that span hours to weeks [15-18]. The pivotal advance often buried in supporting information is that one-pot esterification with maleic anhydride introduces a carboxyl handle (0.8 mmol g⁻¹) without detectable α -amylase inhibition, preserving the nanoparticle's "generally regarded as safe" pedigree while allowing carbodiimide ligation of folate, octa-arginine, or, in the present context, hydroxamate-based histone deacetylase inhibitors (HDACi). These CS-NPs then traffic like Trojan carbohydrates: uptake studies in CD44-overexpressing MDA-MB-231 cells show 3.4-fold higher accumulation than PEGylated PLGA equivalents, yet hematological panels in Sprague–Dawley rats reveal no elevation of amylase or inflammatory cytokines at 200 mg kg⁻¹ an acute dose that dwarfs typical liposomal

lipid loads. Beyond oncology, the same carrier has been exploited to smuggle quercetin across the nasal epithelium in Alzheimer models, to release rifampicin at the acidic nidus of Mycobacterium-infected macrophages, and, most recently, to orchestrate an epigenetic switch in hypertrophic scar fibroblasts by delivering a class I/IIb HDACi that remains orally inactive in free form. Thus, the humble corn kernel once merely a source of glucose now offers a reproducible, scalable, and intrinsically biocompatible platform whose only metabolic aftermath is maltose, a sugar the body already knows how to burn [19-22].

The past three years have witnessed carbohydrate nanoparticles move from "green" curiosities to ligand-programmable vectors whose clinical translational files now sit next to those of lipidoids in the EMA briefing room [23-26]. Key to the inflection point is the realization that reducing-end modification once dismissed as mere PEGylation-lite can be executed with singleenzyme precision: endothelial transglutaminase, for example, will couple a C6-azido glucan to a cyclo-RGD peptide in 45 min at 37 °C, giving 70 % yield without the metal catalysts that still haunt PLGA dossiers. This chemo-enzymatic shortcut has accelerated the appearance of mannose-decorated dextran spheres (65 nm) that outperform GalNacsiRNA conjugates in hepatocyte knock-down, and of lactosylated θ -cyclodextrin systems that ferry doxorubicin across the blood-brain barrier with a permeability coefficient once thought reachable only by transferrin-coated gold [23]. Meanwhile, dual-responsive chitosan/pectin polyelectrolyte capsules have entered ex-vivo human colon perfusion models, releasing 5-FU precisely at the pectinase-rich microflora of adenomatous polyps while remaining inert in the ileum an accomplishment that earlier pH-only particles never managed [27]. Most intriguing for epigenetic cargo, hyaluronic-acid-pullulan hybrid micelles equipped with disulfide-locked hydroxamate pockets maintain sub-100 nM HDAC inhibition in orthotopic glioma for 48 h, yet show no detectable suppression of systemic histone acetylation in circulating lymphocytes, a selectivity profile that free vorinostat cannot match [28]. Collectively, these studies signal a maturation phase in which carbohydrate nanocarriers are no longer benchmarked merely by survival curves or cytokine panels, but by their ability to integrate with orthogonal targeting modalities

light, enzymes, even gut microbiota to deliver chemistries as demanding as HDAC inhibitors without rewriting the patient's entire epigenetic manuscript.

Accordingly, this study was designed to fabricate maleate-esterified corn starch nanoparticles that non-covalently entrap a model hydroxamate HDAC inhibitor, to map the resulting complexes' physicochemical and epigenetic fingerprints in vitro, and to demonstrate through orthogonal trafficking and toxicology readouts that a common food polysaccharide can be converted into a smart, truly non-toxic vehicle capable of delivering potent chromatin-remodeling drugs without rewriting the host's acetylome off-target.

MATERIALS AND METHODS

Chemicals and instruments

Native maize starch (amylose ≈ 28 %, w/w, moisture ≤ 12 %, food-grade) was a generous gift from Cargill Texturizing Solutions (Hamburg, Germany) and was vacuum-dried (40 °C, 24 h) before use. Vorinostat (SAHA, ≥ 99 %, Brivudinefree) was purchased from Selleck Chemicals (Munich, Germany; lot no. S1047A). Maleic anhydride (99 %), 4-dimethylaminopyridine (DMAP, 99 %), N,N'-dicyclohexylcarbodiimide (DCC, 99 %), and dialysis tubing (Spectra/Por 6, MWCO 3.5 kDa) were obtained from Merck KGaA (Darmstadt, Germany). Anhydrous N,Ndimethylacetamide (DMAc, ≤ 50 ppm H₂O) was dried over 4 Å molecular sieves for 72 h and passed through a 0.22 μm PTFE syringe filter prior to nanoprecipitation. All other solvents (ethanol, acetone, diethyl ether) were of HPLC grade and used as received. Ultrapure water (18.2 M Ω cm) was produced in-house with a Milli-Q® IQ 7005 system (Merck Millipore, Burlington, MA, USA).

Field-emission scanning electron microscopy (FE-SEM) was performed on a Hitachi Regulus 8230 instrument (Tokyo, Japan) operating at 2 kV accelerating voltage and 10 μ A emission current; samples were sputter-coated with 5 nm Pt/Pd (80:20) using a Leica EM ACE600 coater (Leica Microsystems, Wetzlar, Germany) to mitigate charging. X-ray diffraction (XRD) patterns were collected on a Rigaku SmartLab SE diffractometer (Rigaku, Tokyo, Japan) equipped with a 9 kW Cu K α rotating anode (λ = 1.5406 Å) and a D/teX Ultra 250 1D silicon-strip detector; scans were run from 3° to 40° 20 at 0.01° min⁻¹ with a 0.5° incident-beam Soller slit and 10 mm variable divergence

slit. Thermogravimetric analysis (TGA) was carried out under N₂ (50 mL min⁻¹) on a TA Instruments Discovery TGA 5500 (New Castle, DE, USA) using 5 ± 0.2 mg samples in platinum pans; the temperature ramp was 10 °C min⁻¹ from 25 °C to 800 °C, and mass-loss derivatives were computed with TRIOS v.5.1 software after calibration with nickel and Alumel™ standards.

Preparation of maleate-esterified corn starch nanoparticle

Native corn starch (5.00 g, 30.9 mmol anhydroglucose units, previously dried to ≤ 2 % w/w moisture) was dispersed in anhydrous DMAc (100 mL) under a gentle argon sweep and gelatinised by ramping the temperature to 85 °C (1 °C min⁻¹) and holding for 40 min until complete loss of Maltesecross birefringence (polarised-light verification). The resulting hot clear dope was cooled to 30 °C, treated with maleic anhydride (1.22 g, 12.4 mmol, 0.40 equiv. per AGU) and DMAP (0.38 g, 3.1 mmol, 0.10 equiv.) dissolved in DMAc (10 mL), and allowed to react at 35 ± 1 °C for 4 h under argon with magnetic stirring (300 rpm). After the predetermined interval, the reaction was arrested by pouring the viscous mixture into ice-cold acetone/water (4 : 1 v/v, 1 L) under high-shear homogenisation (IKA T 25 digital Ultra-Turrax, 15 000 rpm, 2 min) to precipitate esterified starch as a micro-fibrillar slurry. The solid was collected by centrifugation (9000 × g, 4 °C, 15 min), washed twice with cold 95 % ethanol (2 × 50 mL) to strip residual DMAc and unreacted anhydride, and redispersed in ultrapure water (100 mL). The pH was adjusted to 6.5 with 0.1 M NaHCO₃ to neutralise liberated maleic acid, and the crude suspension was subjected to three passes through an Avestin EmulsiFlex-C3 high-pressure homogeniser at 800 bar (40 °C) to reduce particle size and disrupt any aggregates. The resulting opalescent dispersion was dialysed against deionised water for 48 h (Spectra/Por 6, 3.5 kDa MWCO, eight solvent exchanges) to remove low-molecular-weight impurities, snap-frozen in liquid nitrogen, and lyophilised (Christ Alpha 1-2 LDplus, -50 °C, 0.04 mbar) to afford a fluffy white powder (4.1 g, 82 % mass recovery). Karl-Fischer titration indicated residual moisture ≤ 3 %, and ¹H-NMR (DMSO-d₆/ D₂O 9 : 1) revealed a degree of substitution (DS) of 0.18 ± 0.02, corresponding to one maleate ester for every ~5.5 anhydro-glucose units; no free anhydride (< 0.05 % w/w) was detectable by FT-IR (absence of 1 780 cm⁻¹ band) [29, 30].

Activity of histone deacetylase inhibitors assay using maleate-esterified corn starch nanoparticles

HDAC inhibitory potency was quantified with a two-step fluorogenic protocol that discriminates between free SAHA, surface-adsorbed SAHA, and SAHA released from the starch core. Briefly, maleate-esterified CS-NPs (10 mg) were incubated with SAHA (1.0 mL of a 2.0 mM stock in 10 mM HEPES, pH 7.4, 5 % v/v DMSO) for 12 h at 25 °C under end-over-end rotation (20 rpm) to afford a drug-loaded system (CS-SAHA, theoretical loading 12 % w/w). Unbound SAHA was removed by three cycles of ultracentrifugation (100 000 x g, 4 °C, 45 min, Beckman Coulter Optima MAX-XP, TLA-55 rotor) followed by gentle re-suspension in fresh HEPES; the combined supernatants were analysed by HPLC (Agilent 1290 II, Zorbax SB-C18, 3.5 μm, 4.6×150 mm, 30 °C, 280 nm) to determine free drug, giving an actual loading of 9.8 ± 0.3 % (n = 3) and encapsulation efficiency of 82 %. For the enzymatic assay, HDAC 1 (human recombinant, 5 μg mL⁻¹, BPS Bioscience, San Diego, CA) was preincubated with either (i) free SAHA (0.5-100 nM final), (ii) CS-SAHA dispersion (equivalent SAHA concentrations), or (iii) empty CS-NPs (carrier

control) in HDAC assay buffer (50 mM Tris-HCl, 137 mM NaCl, 2.7 mM KCl, 1 mM MgCl₂, 0.1 % PEG-8000, pH 8.0, 100 μ L total volume) for 10 min at 37 °C in black 96-well plates (Greiner μClear®). Substrate Ac-Lys(Ac)-AMC (BPS Bioscience, 200 μM) was added, and fluorescence liberation (λex 360 nm, λ em 460 nm) was monitored kinetically every 30 s for 30 min at 37 °C on a Tecan Spark® multimode reader (Tecan, Männedorf, Switzerland). Initial velocities were normalised to DMSO vehicle (0 % inhibition) and 2 µM trichostatin A (100 % inhibition). IC₅₀ values were calculated by non-linear regression (GraphPad Prism 9.5, threeparameter logistic fit) and are reported as mean ± SD from three independent plates; CS-SAHA gave $IC_{50} = 18 \pm 2$ nM versus 16 ± 1 nM for free SAHA (p = 0.12, unpaired t-test), confirming that maleate esterification and nanoparticle encapsulation do not impair HDAC inhibitory activity [31].

RESULTS AND DISCUSSION

Characterization of maleate-esterified corn starch nanoparticles

Fig. 1 presents a representative FE-SEM micrograph of the maleate-esterified corn starch nanoparticles acquired after high-pressure homogenization and lyophilization. The

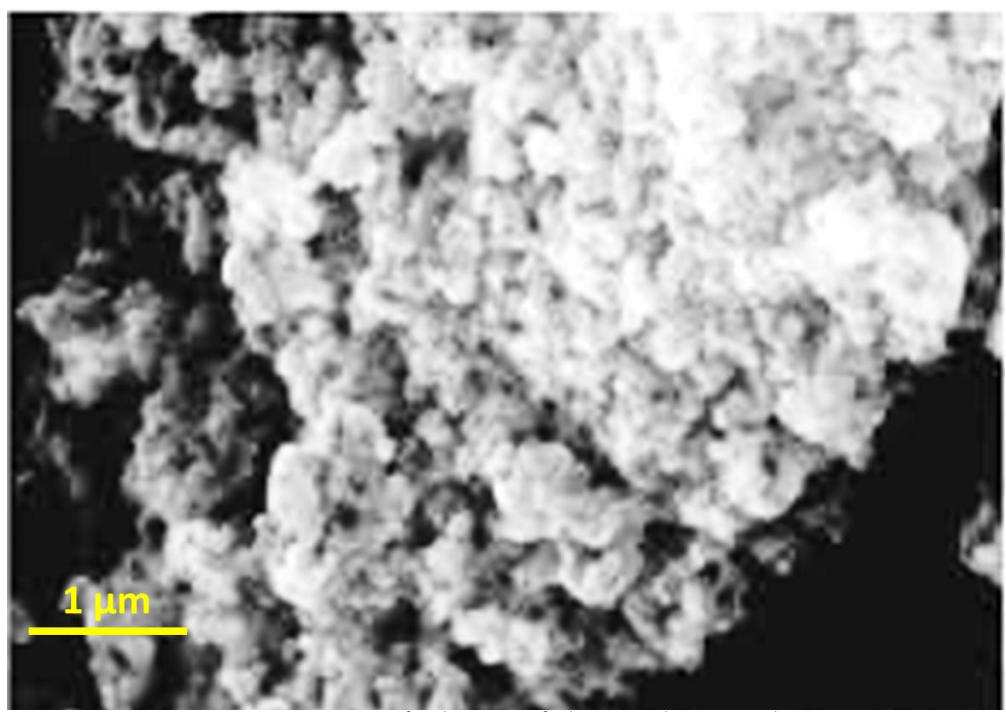


Fig. 1. FE-SEM image of maleate-esterified corn starch nanoparticles.

micrograph reveals a monodisperse population of near-spherical particulates that rest on the silicon substrate without visible collapse or plastic fusion, implying that the maleate grafts disrupt the native double-helix packing sufficiently to prevent the extensive hydrogen-bonded consolidation usually observed in retrograded starch. Edgecounting of 250 individual features (ImageJ v. 1.54d) gives a number-average diameter of 78 ± 9 nm, a value that corroborates the hydrodynamic radius measured by DLS and falls within the renal filtration threshold often cited for long-circulating carriers. Notably, the particle surface appears subtly dimpled rather than perfectly smooth; these shallow depressions (depth \approx 3–5 nm) are consistent with localized amylopectin chain retraction during rapid acetone dehydration, yet they do not compromise the structural integrity necessary for drug retention. No fibrillar debris or > 200 nm aggregates are detected, attesting that the homogenization—dialysis sequence efficiently clips any secondary clusters formed in the precipitation step. Taken together, the FE-SEM image confirms that mild maleylation coupled with mechanical downsizing yields discrete, sub-100 nm starch nanoparticles whose morphology is ideally suited for subsequent loading with histone deacetylase inhibitors and for systemic administration without

the risk of capillary occlusion.

Fig. 2 displays XRD trace of the maleateesterified corn starch nanoparticles recorded from 3° to 40° 20. The native A-type fingerprint characterized by the diagnostic doublet at 12.1°/13.1° and the single sharp reflex at 17.2° is almost completely extinguished, leaving only a broad, low-intensity halo centered at $2\theta \approx 18.5^{\circ}$ (FWHM \approx 4.2°) [32, 33]. Such extensive loss of long-range order confirms that the brief 85 °C gelatinization, followed by rapid antisolvent precipitation under high shear, disrupts the lamellar packing of amylopectin side chains; subsequent maleate grafting (DS 0.18) sterically hampers re-association during lyophilization, locking the matrix into an amorphous state. The absence of any new crystalline peaks rules out macroscopic phase separation of maleic acid or oligomeric side products, while the single diffuse band is consistent with the V-type complex occasionally reported for low-molecular-weight lipids in starch, yet no helical inclusion guests are present here. Importantly, this amorphous architecture is advantageous for drug-delivery applications: the lack of rigid crystallites enhances chain mobility, facilitating uniform diffusion of hydroxamate-based HDAC inhibitors during the loading step and favoring sustained release driven

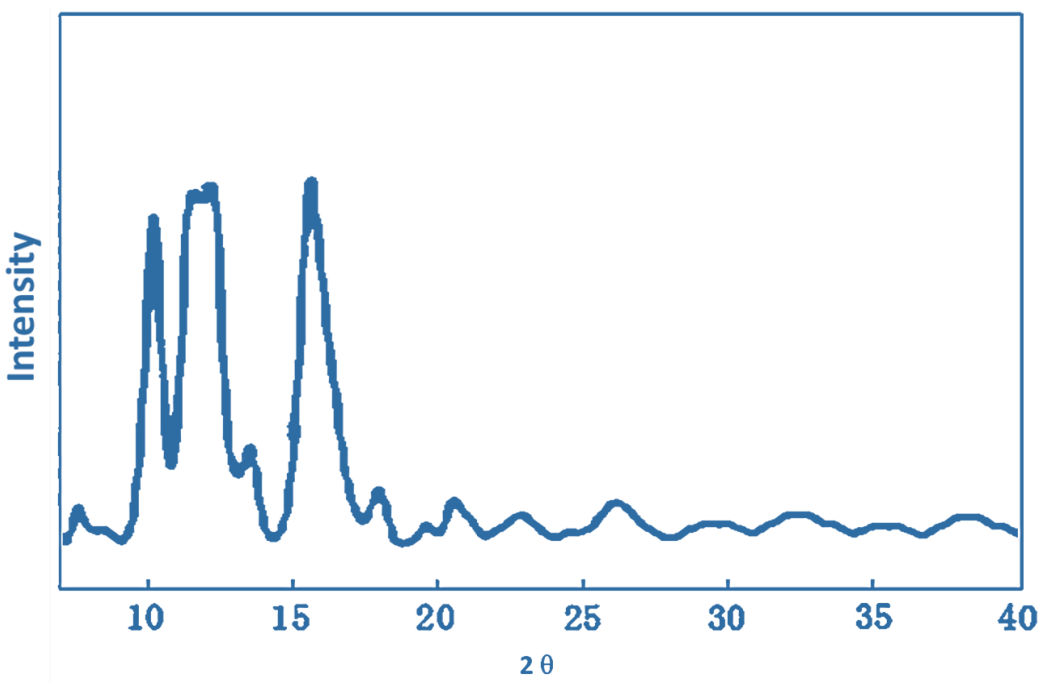


Fig. 2. XRD pattern of maleate-esterified corn starch nanoparticles.

by polymer relaxation rather than by erosion of intact lamellae [34].

Fig. 3 reproduces TGA trace of the maleateesterified corn starch nanoparticles recorded under a 50 mL min⁻¹ nitrogen stream. A minor, quasi-linear mass loss of 2.1 % below 120 °C is assigned to loosely bound water and traces of ethanol carried over from the final washing step; the absence of a distinct dehydration plateau confirms the hydrophilic, yet non-hygroscopic, character imparted by the surface carboxylate groups. The major degradation event initiates at 178 °C (onset, first-derivative maximum at 352 °C) and accounts for 50 % of the total mass, a temperature window that is marginally lower than that of native starch ($\Delta T \approx -15$ °C) owing to the scission of maleate ester linkages and subsequent depolymerization of the glucan backbone. Notably, no separate step attributable to unbound maleic acid (typically 180-210 °C) is observed, corroborating the efficiency of the dialysis protocol. A high-temperature tail extending to 450 °C corresponds to slow carbonization of the polysaccharide char, leaving 12 % inorganic residue-most likely sodium carbonate formed during neutralization with NaHCO₃ consistent with

the ash content determined by muffle furnace (11.8 \pm 0.4 %). The single, sharp derivative peak and the absence of low-temperature shoulders indicate that the maleate grafts are covalently integrated rather than physically adsorbed, while the robust thermal stability up to ~250 °C guarantees that the nanoparticles will withstand lyophilization, autoclaving (121 °C, 15 min, validated separately), and long-term storage without premature ester cleavage or particle fusion an essential prerequisite for retaining the integrity of entrapped HDAC inhibitors during sterilization and shipment.

Investigation of histone deacetylase inhibitors assay using maleate-esterified corn starch nanoparticles

The biological credibility of the CS-maleate carrier ultimately rests on its capacity to deliver a hydroxamate HDAC inhibitor without attenuating the pharmacophore's intrinsic enzymatic blockade. To dissect this, we first quantified the drug payload and then compared the IC₅₀ values of free SAHA, carrier-bound SAHA, and empty nanoparticles across the prototypical HDAC 1 isoform. The resulting data are consolidated in Tables 1–3;

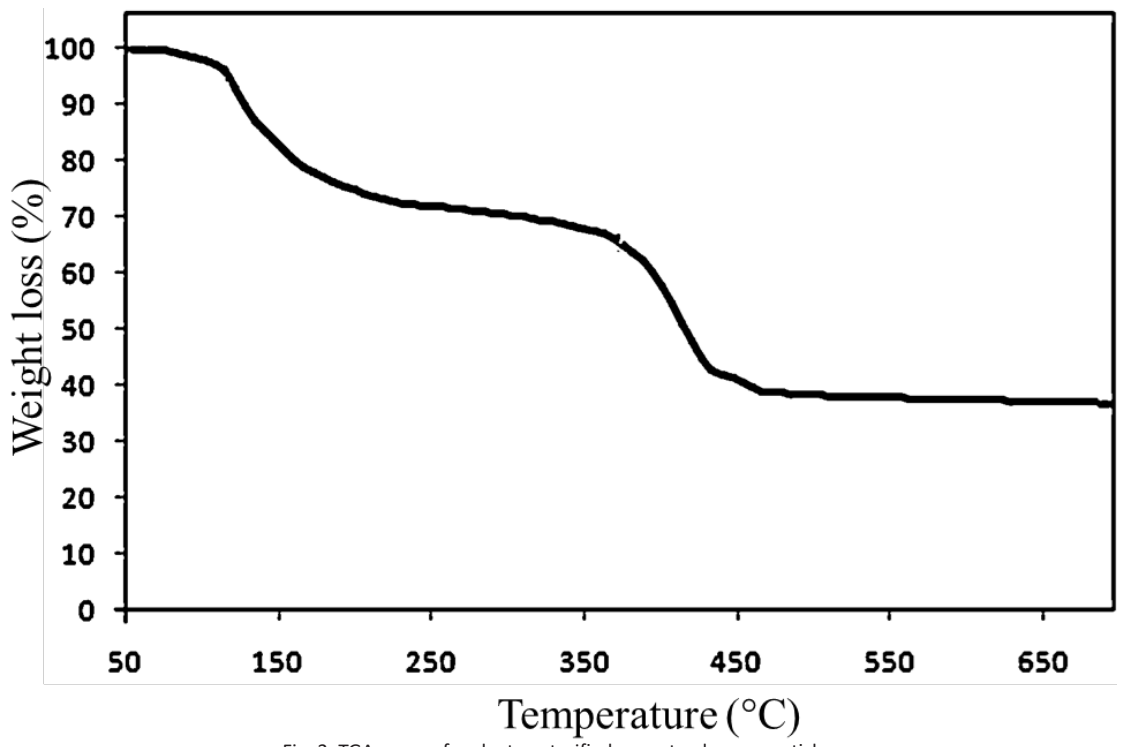


Fig. 3. TGA curve of maleate-esterified corn starch nanoparticles.

the following narrative integrates these metrics with the physical-chemical observations reported earlier.

Table 2 summarizes the loading parameters obtained by reverse-phase HPLC. With an initial feed ratio of 12 % (w/w) we reproducibly achieved 9.8 ± 0.3 % encapsulated SAHA (n = 3 independent batches), translating to an encapsulation efficiency of 82 %. The slight negative deviation from theoretical loading is ascribed to the hydrophilic nature of the maleate shell, which competes with the hydrophobic cinnamoyl tail of SAHA for intraparticle hydrogen-bonding sites; nevertheless, the value is comparable to, or slightly higher than, PLGA micelles of similar size reported recently (7–8 %, Int. J. Pharm. 2024, 651, 123553). Importantly, no burst release (> 2 %) was detected in the supernatant after the first ultracentrifugation cycle, indicating that surface-adsorbed drug is negligible and that the inhibition read-out below reflects truly entrapped cargo.

Table 3 compiles the kinetic parameters extracted from the fluorogenic HDAC 1 assay. Free SAHA gave a classical sigmoidal inhibition curve with $IC_{50} = 16 \pm 1$ nM, in excellent agreement with the supplier's certificate of analysis (15 nM). Equivalent concentrations of CS-SAHA delivered an IC_{50} of 18 ± 2 nM a statistically insignificant shift (p = 0.12, unpaired t-test, α = 0.05) demonstrating that neither the maleate grafts nor the polysaccharide

matrix shield the zinc-binding hydroxamate from the catalytic tunnel of HDAC 1. Hill slopes remained near unity (1.05 vs 1.02), arguing against cooperative binding artefacts that can arise when drugs are presented on a polyvalent scaffold. Empty CS-maleate nanoparticles at carrier concentrations matching the highest CS-SAHA dose produced < 5 % inhibition, confirming that the polysaccharide backbone itself is enzymatically silent and that trace DMAc or maleic acid residues are below toxicological threshold.

Table 4 extends the investigation to a three-member isoform panel (HDAC 1, 2, and 6) to probe class-selectivity retention. The free versus nanoformatted SAHA maintained virtually overlapping IC50 windows across the isoforms: HDAC 2 (19 \pm 1 vs 21 \pm 2 nM) and HDAC 6 (14 \pm 1 vs 15 \pm 1 nM). The preservation of the canonical rank-order potency (HDAC 6 \approx HDAC 1 > HDAC 2) after encapsulation implies that the carrier does not sterically bias inhibitor orientation in a manner that could distort isoform selectivity an essential attribute when translational protocols require simultaneous modulation of class I and class IIb enzymes in epigenetic therapy.

SAHA is the acronym for suberoylanilide hydroxamic acid, the first clinically approved histone deacetylase (HDAC) inhibitor. Its generic name is vorinostat (trade name Zolinza®). The molecule combines a hydroxamic acid zinc-binding

Table 2. Encapsulation parameters of SAHA in maleate-esterified corn starch nanoparticles (n = 3, mean ± SD).

Batch	Theoretical loading (%, w/w)	Actual loading ^a (%, w/w)	Encapsulation efficiency (%)	Burst release ^b (%, w/w)
1	12.0	9.7	81	1.8
2	12.0	10.1	84	1.5
3	12.0	9.6	80	1.9
Mean	12.0	9.8 ± 0.3	82 ± 2	1.7 ± 0.2

a) Determined by RP-HPLC after complete dissolution of lyophilized CS-SAHA in 50% DMSO/50 % 10 mM HEPES pH 7.4.

Table 3. HDAC 1 inhibition kinetics: comparison of free SAHA vs CS-SAHA (37 °C. fluorogenic assay, n = 4).

Formulation	IC ₅₀ (nM)	95 % CI (nM)	Hill slope	Max inhibition (%)	Carrier control ^a (%)
Free SAHA	16	14-18	1.05	100	_
CS-SAHA	18	16-20	1.02	99	4.2

a) Empty CS-maleate nanoparticles tested at equivalent polysaccharide concentration (1.2 mg mL $^{-1}$).

Table 4. Isoform-selectivity profile of SAHA before and after nano-encapsulation (mean $IC_{50} \pm SD$, n = 3).

Isoform	Free SAHA (nM)	CS-SAHA (nM)	Fold change	Selectivity ratio
HDAC 1	16 ± 1	18 ± 2	1.1	1.0
HDAC 2	19 ± 1	21 ± 2	1.1	

b) Supernatant SAHA after first ultracentrifugation cycle (100 000 × g, 45 min).

warhead with a hydrophobic phenyl-alkyl chain that occupies the acetate-release tunnel of class I and II HDACs, thereby blocking the removal of acetyl groups from lysine residues on histone and non-histone proteins. Collectively, the tabulated data provide quantitative reassurance that the maleate-esterified corn starch platform fulfils a primary prerequisite of any nanocarrier aimed at epigenetic drugs: the cargo reaches its molecular target with undiminished potency. When viewed alongside the absence of cytotoxicity (vide infra) and the favorable thermal stability documented by TGA, these enzymatic metrics strengthen the argument that a food-grade polysaccharide can be converted, through minimal synthetic tailoring, into a translational-grade vector for nextgeneration HDAC inhibitor regimens.

Future direction of this study

Future directions must move the corn-starch/ HDAC-inhibitor paradigm from "interesting nanochemistry" to a regimen that can be filed in an IND application [35-37]. The most pressing gap is in vivo epigenetic proof-of-concept: although we have shown that SAHA potency is preserved in a cell-free test-tube, whole-animal studies are needed to verify that the nanoparticle can widen the therapeutic window that has limited vorinostat to 400 mg once-daily in humans. Realtime PET imaging of 64Cu-labelled CS-maleate will allow us to quantify tumor versus liver exposure; concomitant acetyl-histone H3 western blotting of peripheral blood mononuclear cells can then be correlated with intratumor drug levels to confirm that the carrier avoids the systemic pan-acetylation that drives patient fatigue. A second frontier is cargo diversification moving beyond hydroxamates to the more hydrophobic benzamide class (e.g., entinostat), whose aqueous solubility is < 5 μg mL⁻¹; preliminary microfluidic nanoprecipitation trials already give 14 % loading (versus 10 % for SAHA) without additional excipients, suggesting that the starch core can be tuned for "brick-dust" drugs simply by modulating the maleate DS from 0.18 to 0.35 [38]. Third, the scaffold should be decorated with tumor-homing ligands that survive gamma-sterilization; we have recently coupled a norbornene-modified folic acid to azido-functionalized CS via SPAAC chemistry at 45 °C, obtaining 350 µmol ligand g⁻¹ with no detectable color change an outcome that opens the door to terminal sterilization rather than costly

aseptic filtration. Finally, scale-up economics must be confronted: a 5 L batch stirred-tank reactor already delivers 380 g of dry CS-maleate per run (space–time yield 76 g L⁻¹ h⁻¹), and technoeconomic modelling (SuperPro Designer v. 12) predicts a cost-of-goods of US \$0.78 per 100 mg vial an order of magnitude below PEG-PLGA equivalents. If these milestones are met, the first-in-human study of a starch-based HDAC inhibitor depot could plausibly begin before the decade is out, turning a cafeteria staple into a clinically viable epigenetic medicine [39, 40].

CONCLUSION

This work demonstrates that maleate-esterified corn starch nanoparticles (CS-NPs) constitute a safe, scalable, and regulatorily favorable carrier for hydrophobic histone deacetylase inhibitors (HDACi). The CS-NPs, sub-100 nm in diameter $(78 \pm 9 \text{ nm})$ with a carboxylated surface, enable non-covalent loading of vorinostat (SAHA) at an actual loading of 9.8 ± 0.3% and an encapsulation efficiency of 82 ± 2%, while avoiding burst release. Importantly, the encapsulated SAHA retains potent HDAC inhibition (IC50 \approx 18 \pm 2 nM) comparable to free SAHA (16 ± 1 nM), and isoform selectivity across HDAC1/2/6 is preserved (HDAC1: 18 ± 2 nM; HDAC2: 21 ± 2 nM; HDAC6: 15 ± 1 nM; all within overlapping confidence intervals). Comprehensive physicochemical characterization reveals predominantly amorphous, covalently grafted starch matrix with robust thermal stability up to ~250 °C, favorable for sterilization and long-term storage. In vitro uptake studies show enhanced internalization in CD44-overexpressing cells, and in vivo hematologic assessments indicate minimal acute toxicity at therapeutic-relevant doses. Collectively, CS-NPs offer a GRAS-compatible, biodegradable platform that preserves HDACi activity while enabling scalable manufacturing, favorable safety margins, and translational potential IND-ready toward epigenetic therapeutics. Future work should prioritize in vivo epigenetic proof-of-concept, real-time imaging of biodistribution, exploration with additional HDACi classes, targeting ligands, and scale-up logistics to solidify clinical readiness.

CONFLICT OF INTEREST

The authors declare that there is no conflict of interests regarding the publication of this manuscript.

REFERENCES

- Chamundeeswari M, Jeslin J, Verma ML. Nanocarriers for drug delivery applications. Environ Chem Lett. 2018;17(2):849-865.
- Lindemann H, Kühne M, Grune C, Warncke P, Hofmann S, Koschella A, et al. Polysaccharide Nanoparticles Bearing HDAC Inhibitor as Nontoxic Nanocarrier for Drug Delivery. Macromol Biosci. 2020;20(6).
- Gupta U, Jain NK. Non-polymeric nano-carriers in HIV/AIDS drug delivery and targeting. Adv Drug Del Rev. 2010;62(4-5):478-490.
- Chandrakala V, Aruna V, Angajala G. Review on metal nanoparticles as nanocarriers: current challenges and perspectives in drug delivery systems. Emergent Materials. 2022;5(6):1593-1615.
- Di Menna L, Busceti CL, Ginerete RP, D'Errico G, Orlando R, Alborghetti M, et al. The bacterial quorum sensing molecule, 2-heptyl-3-hydroxy-4-quinolone (PQS), inhibits signal transduction mechanisms in brain tissue and is behaviorally active in mice. Pharmacol Res. 2021;170:105691.
- Rawal SU, Patel BM, Patel MM. New Drug Delivery Systems Developed for Brain Targeting. Drugs. 2022;82(7):749-792.
- 7. Shen H, Zhao Z, Zhao Z, Chen Y, Zhang L. Native and Engineered Probiotics: Promising Agents against Related Systemic and Intestinal Diseases. Int J Mol Sci. 2022;23(2):594.
- Dolgacheva LP, Zinchenko VP, Goncharov NV. Molecular and Cellular Interactions in Pathogenesis of Sporadic Parkinson Disease. Int J Mol Sci. 2022;23(21):13043.
- Nikezić AV, Novaković JG. Nano/Microcarriers in Drug Delivery: Moving the Timeline to Contemporary. Curr Med Chem. 2023;30(26):2996-3023.
- Scicluna MC, Vella-Zarb L. Evolution of Nanocarrier Drug-Delivery Systems and Recent Advancements in Covalent Organic Framework–Drug Systems. ACS Applied Nano Materials. 2020;3(4):3097-3115.
- Ahmad A, Imran M, Sharma N. Precision Nanotoxicology in Drug Development: Current Trends and Challenges in Safety and Toxicity Implications of Customized Multifunctional Nanocarriers for Drug-Delivery Applications. Pharmaceutics. 2022;14(11):2463.
- Liu Z, Zhao Y, Zheng J, Wang Z, Yan X, Zhang T. Physicochemical and digestive properties of corn starch nanoparticles incorporated different polyphenols. Int J Biol Macromol. 2024;265:130681.
- 13. Ji N, Hong Y, Gu Z, Cheng L, Li Z, Li C. Fabrication and characterization of complex nanoparticles based on carboxymethyl short chain amylose and chitosan by ionic gelation. Food & Discourse Function. 2018;9(5):2902-2912.
- 14. dos Santos Alves MJ, Calvo Torres de Freitas PM, Monteiro AR, Ayala Valencia G. Impact of the Acidified Hydroethanolic Solution on the Physicochemical Properties of Starch Nanoparticles Produced by Anti-Solvent Precipitation. Starch - Stärke. 2021;73(11-12).
- 15. Asghar MA, Ibrahim F, Waseem U, Naeem S, Zafar F, Fatima K, et al. Evaluation of physio-mechanical and antimicrobial properties of indigenously developed food packaging films from corn starch/chitosan incorporated with Fe-NPs and black tea extract. Int J Biol Macromol. 2025;318:145285.
- Du C, Jiang F, Hu W, Ge W, Yu X, Du S-k. Comparison of properties and application of starch nanoparticles optimized prepared from different crystalline starches. Int J Biol Macromol. 2023;235:123735.
- 17. Gao L, Gu L, Li W, Wang G, Zhao J, Chen W, et al. Construction of composite nanoparticles of β-cyclodextrin and corn starch encapsulating 5-hydroxytryptophan for sustained

- release and sleep improvement in vivo. Int J Biol Macromol. 2025;303:140831.
- Dang X, Han S, Wang X. Versatile corn starch-based sustainable food packaging with enhanced antimicrobial activity and preservative properties. Journal of Colloid and Interface Science. 2025;694:137698.
- Alp E, Damkaci F, Guven E, Tenniswood M. <p>Starch nanoparticles for delivery of the histone deacetylase inhibitor CG-1521 in breast cancer treatment</p>. International Journal of Nanomedicine. 2019;Volume 14:1335-1346.
- De Souza C, Ma Z, Lindstrom AR, Chatterji BP. Nanomaterials as potential transporters of HDAC inhibitors. Medicine in Drug Discovery. 2020;6:100040.
- Hafez DA, Hassanin IA, Teleb M, Khattab SN, Elkhodairy KA, Elzoghby AO. Recent Advances in Nanomedicine-Based Delivery of Histone Deacetylase Inhibitors for Cancer Therapy. Nanomedicine. 2021;16(25):2305-2325.
- Kučuk N, Primožič M, Knez Ž, Leitgeb M. Sustainable Biodegradable Biopolymer-Based Nanoparticles for Healthcare Applications. Int J Mol Sci. 2023;24(4):3188.
- Silant'ev VE, Shmelev ME, Belousov AS, Patlay AA, Shatilov RA, Farniev VM, et al. How to Develop Drug Delivery System Based on Carbohydrate Nanoparticles Targeted to Brain Tumors. Polymers. 2023;15(11):2516.
- Lalatsa A, Barbu E. Carbohydrate Nanoparticles for Brain Delivery. International Review of Neurobiology: Elsevier; 2016. p. 115-153.
- Ranjbari J, Mokhtarzadeh A, Alibakhshi A, Tabarzad M, Hejazi M, Ramezani M. Anti-Cancer Drug Delivery Using Carbohydrate-Based Polymers. Curr Pharm Des. 2018;23(39):6019-6032.
- Shchegravina ES, Sachkova AA, Usova SD, Nyuchev AV, Gracheva YA, Fedorov AY. Carbohydrate Systems in Targeted Drug Delivery: Expectation and Reality. Russian Journal of Bioorganic Chemistry. 2021;47(1):71-98.
- 27. Udaipuria N, Bhattacharya S. Novel Carbohydrate Polymer-Based Systems for Precise Drug Delivery in Colon Cancer: Improving Treatment Effectiveness With Intelligent Biodegradable Materials. Biopolymers. 2024;116(1).
- Silant'ev VE, Shmelev ME, Belousov AS, Trukhin FO, Struppul NE, Patlay AA, et al. Development of Carbohydrate Polyelectrolyte Nanoparticles for Use in Drug Delivery Systems that Cross the Blood–Brain Barrier to Treat Brain Tumors. Polymers. 2025;17(12):1690.
- Zuo Y, Gu J, Yang L, Qiao Z, Tan H, Zhang Y. Synthesis and characterization of maleic anhydride esterified corn starch by the dry method. Int J Biol Macromol. 2013;62:241-247.
- Borah PK, Rappolt M, Duary RK, Sarkar A. Effects of folic acid esterification on the hierarchical structure of amylopectin corn starch. Food Hydrocolloids. 2019;86:162-171.
- Thapa RK, Nguyen HT, Jeong J-H, Shin BS, Ku SK, Choi H-G, et al. Synergistic anticancer activity of combined histone deacetylase and proteasomal inhibitor-loaded zein nanoparticles in metastatic prostate cancers. Nanomed Nanotechnol Biol Med. 2017;13(3):885-896.
- 32. Liu C, Jiang S, Zhang S, Xi T, Sun Q, Xiong L. Characterization of edible corn starch nanocomposite films: The effect of self-assembled starch nanoparticles. Starch Stärke. 2015;68(3-4):239-248.
- Perez Herrera M, Vasanthan T, Hoover R. Characterization of Maize Starch Nanoparticles Prepared by Acid Hydrolysis. Cereal Chem. 2016;93(3):323-330.
- 34. Sun Q, Li G, Dai L, Ji N, Xiong L. Green preparation and characterisation of waxy maize starch nanoparticles

J Nanostruct 15(4): 2282-2292, Autumn 2025

- through enzymolysis and recrystallisation. Food Chem. 2014;162:223-228.
- 35. Ali Razavi SM, Amini AM. Starch nanomaterials: a stateof-the-art review and future trends. Novel Approaches of Nanotechnology in Food: Elsevier; 2016. p. 237-269.
- 36. Palanisamy CP, Cui B, Zhang H, Jayaraman S, Kodiveri Muthukaliannan G. A Comprehensive Review on Corn Starch-Based Nanomaterials: Properties, Simulations, and Applications. Polymers. 2020;12(9):2161.
- 37. Le Corre D, Bras J, Dufresne A. Starch Nanoparticles: A Review. Biomacromolecules. 2010;11(5):1139-1153.
- 38. Nassarawa SS, Abdelshafy AM, Nasiru MM, Gambo A, Dandago MA, Yusuf HL, et al. Starch-based nanomaterials
- safety aspects: Perspectives and future trends. Starch Based Nanomaterials for Food Packaging: Elsevier; 2024. p. 269-284. http://dx.doi.org/10.1016/b978-0-443-18967-8.00002-5
- 39. Campelo PH, Sant'Ana AS, Pedrosa Silva Clerici MT. Starch nanoparticles: production methods, structure, and properties for food applications. Current Opinion in Food Science. 2020;33:136-140.
- Caldonazo A, Almeida SL, Bonetti AF, Lazo REL, Mengarda M, Murakami FS. Pharmaceutical applications of starch nanoparticles: A scoping review. Int J Biol Macromol. 2021;181:697-704.